Applied Chemical Engineering (2026) Volume 9 Issue 3 ISSN: 2578-2010 (O)
doi: 10.59429/ace.v9i3.6151

RESEARCH ARTICLE

Synthesis and characterization of new thiadiazole ligand and its Co(II), Ni(II), and Cu(II) complexes: Cyclic voltammetry (CV) and preliminary in vitro evaluation of the free ligand

Noor Lateef Kadim*, Zainab Majed Kareem

Department of Chemistry, College of Science, University of Thi-Qar, Thi-Qar 64001, Iraq

***Corresponding author:** Noor Lateef Kadim, noor.lateef@utq.edu.iq

ABSTRACT

The thiadiazole-based ligand (L_1) and its Co(II), Ni(II), and Cu(II) complexes were synthesized and characterized using physicochemical methods, as well as supported by various spectroscopic techniques. FT-IR and UV–Visible spectroscopy, along with molar conductivity studies, supported the intended mode of coordination of ligands with metal ions and authenticated the proposed geometry of the complexes. Cyclic voltammetry studies were carried out to get an insight into the redox properties of the synthesized complexes. The redox couples were assigned, and reversibility of the reaction was assessed by calculating various electrochemical parameters like the ratio of anodic- to cathodic peak current (Ipa/Ipc) and peak potential difference (ΔEp). Results showed that the metal complexes displayed encouraging redox features, which are indicative of metal influence on the ligand electron attributes. Preliminary in vitro cytotoxicity screening of the free ligand L_1 was performed against HBL-100 human breast epithelial cells and the MCF-7 breast cancer cells. Compound L_1 did not reach 50% inhibition at the tested concentrations (15, 30, and 45 µg/mL); therefore, the IC_{50} value was not determined under the experimental conditions.

Keywords: 1,3,4- thiadiazole; metal complexes; spectroscopic characterization; cyclic voltammetry (CV); molar conductivity; anticancer activity; electron density distribution

ARTICLE INFO

Received: 27 August 2026
Accepted: 24 September 2026
Available online: 29 October 2026

COPYRIGHT

Copyright © 2026 by author(s).
Applied Chemical Engineering is published by Arts and Science Press Pte. Ltd. This work is licensed under the Creative Commons Attribution-NonCommercial 4.0 International License (CC BY 4.0).
https://creativecommons.org/licenses/by/4.0/

1. Introduction

Heterocyclic compounds are of major importance in medicine and in pharmaceutical chemistry, primarily due to their structural diversity, but also due to their wide range of biological activities, which is quite significant for research and treatment[1,2]. Among the most significant are the thiadiazole ring and, in particular, the 1,3,4-thiadiazole isomer[3], which is one of the most important sulfur-containing five-membered ring systems in the field of rational drug design[4,5]. The great interest in the 1,3,4-thiadiazole ring stems from its bioisostericity to the pyrimidine ring, which forms the structural basis of the three nitrogenous bases that make up DNA. This gives derivatives of this ring the ability to interfere with DNA replication processes. Furthermore, the mesoionic behavior of this ring grants it the ability to penetrate biofilms and interact with target proteins with high efficiency[6,7]. Numerous studies have demonstrated that thiadiazole derivatives constitute an important class of heterocyclic compounds owing to their wide spectrum of biological activities, including antibacterial, antifungal, anti-inflammatory, antiviral, anticonvulsant, and antioxidant activities, in addition to anticancer activity, which is a highly active area of research in this context due to the increasing global

burden of cancer, as reported by the World Health Organization[7]. Additionally, the reaction of organic ligands containing donor atoms such as sulfur and nitrogen, as is the case with thiadiazole derivatives, with transition metal ions such as cobalt, nickel, and copper often yields the formation of coordination complexes with distinct physicochemical and biological properties compared with free ligands. Coordination of organic ligands containing donor atoms with transition metal ions can modify their structural, electronic, and physicochemical properties compared with the corresponding free ligands[8]. Moreover, cyclic voltammetry is an analytical technique that is useful to study the electrochemical behavior of such complexes so as to elucidate the redox processes and the electron-transfer mechanism at the metal core. This method gives firm information about the stability of different oxidation states of the metal and reversibility of the electrochemical process[9,10]. The present study aimed to synthesize and characterize a new thiadiazole-derived ligand (L_1) and its complexes with cobalt(II), nickel(II), and copper(II) ions; to investigate their electrochemical behavior using cyclic voltammetry; to evaluate the electron density distribution of the ligand (L_1); and to conduct a preliminary cytotoxicity assessment of the free ligand (L_1) against MCF-7 and HBL-100 cells.

In light of the findings obtained, Jain et al. (2013)[4] performed an extensive review of derivatives of the 1,3,4-thiadiazole scaffold, showing that this heterocyclic ring is present in various clinically used drugs and possesses antimicrobial, anticancer, and anti-inflammatory effects, making it a promising pharmacophore for the discovery of novel therapeutic agents. In a later review, Hu et al. (2014)[5] reviewed the synthetic methods for 1,3,4-thiadiazole derivatives and highlighted their importance in medicinal chemistry, agricultural, and materials chemistry, highlighting the ring's structural versatility and its potential for structural modification to suit diverse biological purposes. Similarly, Li et al. (2013)[6] indicated that the thiadiazole ring represents a promising structure in modern medicinal chemistry due to its wide range of biological activities. More specifically focusing on the anticancer aspect, Indelicato et al. (2025)[7] presented a recent review highlighting the latest developments in the use of 1,3,4-Thiadiazole derivatives, which have emerged as promising molecular scaffolds for the discovery and optimization of novel anticancer compounds, including those targeting breast cancer and pancreatic ductal adenocarcinoma. The review also examined the role of molecular factors in determining the biological behavior of these derivatives. Obakachi et al. (2021)[11] also presented a similar review focusing on the synthetic aspects and anticancer activity of thiadiazole compounds, emphasizing the important role of the sulfur atom in the ring in z enhancing cellular permeability and biological selectivity. In a direct experimental study, Janowska et al. (2022)[12] reported the synthesis of novel 1,3,4-thiadiazole derivatives and investigated their biological activity against cancer cells. Biological evaluation was performed against two representative human breast cancer cell lines with different estrogen receptor profiles, including MCF-7 (ER-positive) and MDA-MB-231 (ER-negative), to investigate the compounds' anticancer potential, compared to a normal human cell line (fibroblasts). The results indicated that several derivatives exhibited significant anticancer activity and selectivity in inhibiting cancer cells without significantly affecting normal cells, supporting the hypothesis that this ring could serve as a baseline structure for developing anti-breast cancer agents. At the level of transition metal complexes, Daravath et al. (2017)[8] conducted a study to prepare copper-cobalt-nickel binary complexes with Schiff base ligands derived from benzothiazole. They characterized these complexes spectroscopically and investigated their interaction with DNA and biological activity. The greater biological activity of the metal complexes compared with the free ligands may be attributed to the chelation effect, which can improve lipophilicity and facilitate cellular uptake, supporting the chelation theory in explaining the enhanced biological activity following metal-coupled interaction. From an electrochemical viewpoint, Kuate et al. (2020)[9] examined the electrochemical behavior of cobalt, nickel, and copper complexes with a three-tooth Schiff base-derived ligand through cyclic voltammetry analysis. They found that the Co(II) and Cu(II) systems displayed quasi-reversible behavior with a single-electron transfer process, while the Ni(III)/Ni(II) system displayed irreversible electrochemical behavior. They further investigated the antibacterial, antifungal, and antioxidant activity of these complexes. Similarly, Venkatesh et al. (2024)[10] used cyclic voltammetry to study the electrochemical properties of metal Schiff base complexes,

along with spectroscopic characterization, theoretical calculations (DFT), and biological activity, including antioxidant and antimicrobial activity. An examination of earlier studies shows that most studies focused on either the spectral and biological aspects of thiadiazole complexes or other similar cyclic compounds, or the electrochemical behavior of Schiff base complexes in general, while only a limited number of studies combined the complete spectral characterization, the electrochemical properties by cyclic voltammetry, and the anti-breast cancer activity specifically, for the same ligand system and its complexes with cobalt, nickel, and copper in one integrated research framework, a gap addressed in the present work. Based on the foregoing, although numerous thiadiazole have been studied due to their structural diversity and significant biological properties still some important points have not been sufficiently addressed. In fact, only synthesis and spectroscopic studies of these compounds were undertaken in most cases. However, comparatively little attention has been given to correlating structural characterization with electrochemical investigations and bioactivity evaluation within one integrated investigation.

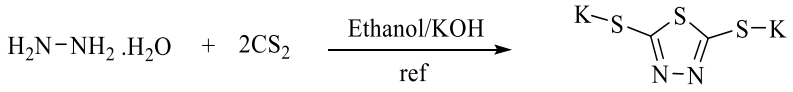
Particularly, the connection between the electrochemical performance of thiadiazole metal complexes and their biological activity remains inadequately understood. The electrochemical characteristics of metal complexes affect their stability, ability to transfer electrons, and interactions with biological targets. Therefore, finding relationships between cyclic voltammetric parameters and anticancer activity could give insight into potential mechanisms of action. Even so, such correlations have only rarely been addressed in previous investigations[13,14]. Moreover, comparative investigations involving Co(II), Ni(II), and Cu(II) thiadiazole-based complexes coordinated with the same thiadiazole ligand under identical experimental conditions are scarce. Therefore, the role of the coordinated metal ion in governing the structural, electrochemical, and biological properties of these complexes has not yet been fully elucidated. Besides, numerous thiadiazole derivatives have been evaluated for their activity against many cancer cell lines, but no work has been reported on the activity of such derivatives against the HBL-100 breast epithelial cell line. This demonstrates the need for further investigation to assess the biological potential of these complexes and to investigate the potential correlation between their molecular structure, redox properties, and their anti-proliferative activity. Thus, the present work aims to fill these gaps by synthesizing new thiadiazole-based Co(II), Ni(II), and Cu(II) complexes and subsequently scrutinising the spectroscopic properties and electrochemical behaviour of these complexes by cyclic voltammetry. In addition, a preliminary cytotoxicity assessment of the free ligand L_1 was carried out against the MCF-7 and the HBL-100 breast epithelial cell line. Overall, this integrated approach should provide a broader kind of insight into how coordination chemistry, redox characteristics, and biological performance connect together, almost like one influencing the other.

2. Materials and methods

2.1. Preparation of 5-Hydrazinyl-1,3,4-thiadiazol-2-amine

Step 1: Preparation of Dipotassium 1,3,4-thiadiazole-2,5-bis(thiolate)

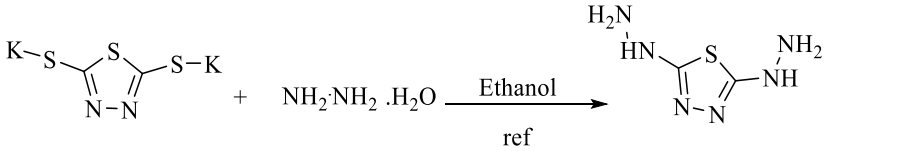
Potassium hydroxide (11.2 g, 0.2 mol) was taken up in ethanol (50 mL) and transferred to a 100 mL round-bottom flask. Hydrazine hydrate (5 mL, 0.1 mol) was then added, and the reaction mixture was heated until complete dissolution was achieved. After dissolution, the mixture was subjected to cooling in an ice bath to approximately 5 °C. Carbon disulfide (15.2 mL, 0.2 mol) was subsequently added portionwise, and the reaction mixture was refluxed for 20 h. The progress and completion of the reaction were monitored by the cessation of hydrogen sulfide gas evolution using lead acetate solution as an indicator. Once the reaction was complete, the reaction mixture was concentrated to approximately half of its original volume, and the resulting precipitate was allowed to cool gradually to room temperature. The crude product was then recrystallized from ethanol to afford pale yellow needle-shaped crystals of dipotassium 1,3,4-thiadiazole-2,5-bis(thiolate)[15]. The product exhibited a melting point of 260–262 °C and was obtained in an 89% yield, as illustrated in **Scheme 1**.



potassium 1,3,4-thiadiazole-2,5-bis(thiolate)

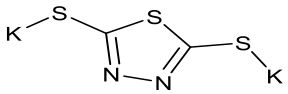
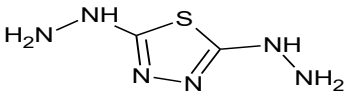
Step 2: Reaction with Hydrazine Hydrate ($NH_2NH_2.H_2O$)

Compound A (10 g, 0.1 mol) was reacted with hydrazine hydrate (8 mL, 0.2 mol) in a 100 mL round-bottom flask using ethanol (50 mL) as the reaction solvent. The reaction was conducted under reflux for 25 h, while its progress was followed by detecting the evolution of hydrogen sulfide gas using a filter paper impregnated with lead acetate solution, which turned black upon exposure to the gas. After completion of the reaction, the resulting precipitate was collected by filtration to afford Compound B as an off-white (yellowish-white) solid. The product exhibited a melting point of 199–201 °C and was obtained in an 83% yield, as shown in **Scheme 2**[16,17]. **Table 1** provides information about compounds A and B.



2,5-dihydrazineyl-1,3,4-thiadiazole

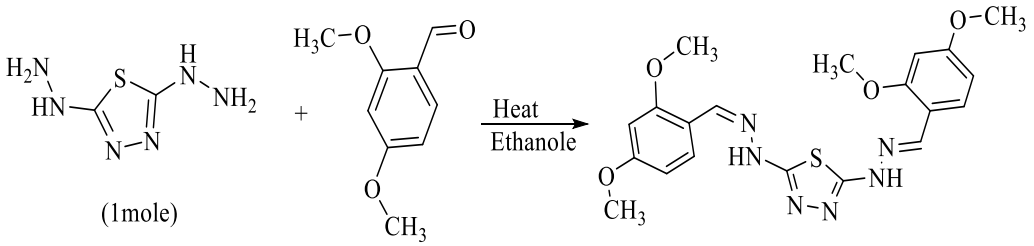
Table 1. Molecular formula, structural formula, and selected physical properties of the synthesized compounds.

Compound	Formula	M. wt	Color	M. pc	Yield%	Rf
	$C_2N_2S_3K_2$	226	Pale Yellow	260-262	89	0.69
	$C_2H_6N_6S$	146	Off-white	199-201	83	0.77

2.2. Preparation of ligand L_1

The ligand was synthesized by the reaction of Compound B (1.5 g, 0.0102 mol) with aldehyde (L_1) using a 1:2 molar ratio of Compound B to 2,4-dimethoxybenzaldehyde.

Compound B was mixed with 2,4-dimethoxybenzaldehyde (2.78 g) using a 100 mL round-bottomed reaction flask, and the reaction mixture was solubilized in ethanol (60 mL)[18]. The course of the reaction was monitored by TLC with ethyl acetate/hexane as the developing solvent (3:7, Rf value). Once the reaction was complete after 8 h, the resulting mixture was cooled and filtered. The obtained precipitate was recrystallized from ethanol[19] to yield dark yellow crystals. The synthesized ligand exhibited a melting point of 213–215 °C and was obtained in a 71% yield, as shown in **Scheme 3**.



2-(2-((E)-2,4-dimethoxybenzylidene)hydrazineyl)-5-(2-((Z)-2,4-dimethoxybenzylidene)hydrazineyl)-1,3,4-thiadiazole

2.3. Preparation of metal complexes

The Co(II), Ni(II), and Cu(II) complexes were prepared through the complexation reaction of the corresponding metal ions with the synthesized ligand in a 1:1 molar ratio (metal: ligand), as described below. In a 50 mL round-bottom flask, the ligand (L_1) (1 mmol), dissolved in ethanol (30 mL), was mixed separately with 1 mmol of the corresponding transition metal salts. The complexation reaction mixtures were refluxed under continuous stirring for 2–3 h, and the progress of the reactions was monitored by thin-layer chromatography (TLC). After completion of the complexation reactions, the mixtures were allowed to cool, resulting in the formation of colored precipitates[20]. The precipitated complexes were filtered off and washed with distilled water to remove any excess metal salts. The physical properties of the prepared complexes, like the molecular formulas, the amounts of ligand and metal salts used, and the yields from the final complexation reactions, can be found in **Table 2** below.

Table 2. Molecular formulas and selected physical properties of ligand L_1 and its metal complexes.

NO.	Formula	M.wt	color	M.pc	Yield %
L_1	$C_{20}H_{22}N_6SO_4$	442	Dark Yellow	213-215	71
1	[Co(L_1)Cl_2.2H_2O]	608	Brown	225-228	87.5
2	[Ni(L_1)Cl_2] 2H_2O	608	Gold	220-222	62.5
3	[Cu(L_1)Cl_2]2H_2O	613	Yellow	230-232	73.9

2.4. Ultraviolet–visible spectroscopy (UV–Vis)

The electronic absorption spectra of the synthesized ligands and their corresponding metal complexes were documented using a UV–Visible spectrophotometer at ambient temperature. Solutions of all compounds at a concentration of 1×10^{-4} mol L^{-1} were produced by dissolving the accurately calculated mass of each compound, based on its molar mass, in N,N-dimethylformamide (DMF) using a polymer tube. The solution volume was made up to 3 mL, followed by thorough mixing to promote complete solubilization and the formation of a homogeneous solution[21] . Before spectral measurements, the prepared solutions were transferred into a 1 cm quartz cuvette. The instrument was standardized using DMF as the blank solution, after which the absorption spectra were measured over the wavelength range of 200–800 nm. The maximum absorption wavelength (λmax) together with the corresponding absorbance values were extracted for each compound. The mass required for preparing each solution was calculated using the following equation, and the corresponding values were listed in **Table 3**.

Mass (grams) = Concentration (mol/L) × Molar mass (g/mol) × Volume (L).

Table 3. The mass of ligand and metal complexes for ultraviolet–visible spectroscopy.

Comp.	L_1	CoL_1	NiL_1	CuL_1
Mass (g)	0.00013	0.00018	0.00017	0.00018

2.5. Molar electrical conductivity

The molar electrical conductivity of the synthesized ligand and its corresponding metal complexes was measured using a conductivity meter at ambient laboratory temperature. Prior to measurements, the conductivity meter was calibrated using a standard potassium chloride (KCl) solution, and the cell constant was determined to be 5.152 cm^{-1}. The solutions of all investigated compounds were prepared at a concentration of 1×10^{-3} $mol.L^{-1}$ using dimethylformamide (DMF) as the solvent. The required mass of each compound was calculated and accurately weighed according to its molecular weight. Afterwards, the weighed samples were placed in polymer tubes and dissolved in DMF. The volume was brought up to 10 mL, and the solutions were well stirred to get complete dissolution and homogeneity of the solution. After the instrument had been calibrated, the conductivity electrode was immersed into each prepared solution, and the electrical conductivity values were recorded[22]. The molar electrical conductivity values of the synthesized compounds were then calculated from the obtained conductivity measurements. The required masses were calculated using the previously described UV equation, and the results are presented in **Table 4.**

Table 4. The mass of ligand and metal complexes for molar electrical conductivity.

Comp.	L_1	CoL_1	NiL_1	CuL_1
Mass (g)	0.004	0.006	0.005	0.006

2.6. Cyclic voltammetry (CV)

Cyclic voltammetry (CV) measurements were carried out using a PARSTAT4000 POTENTIOSTAT/GA

LVANOSTAT/EIS ANALYSER (AMETEK, France) under an inert atmosphere, where a continuous flow of argon gas was maintained at room temperature. The electrochemical measurements were performed in the Department of Chemistry, College of Science, University of Thi-Qar. A conventional single-compartment three-electrode electrochemical cell was employed for all cyclic voltammetric experiments. Tetrabutylammonium perchlorate (TBAP) was utilized as a supporting electrolyte in an anhydrous dimethylformamide (DMF) medium at a concentration of 0.1 M. A freshly polished glassy carbon disk electrode (3 mm diameter) was used as the working electrode for recording the cyclic voltammograms. All CV experiments were performed at a potential scan rate of 100 mV s^{-1}[23]. The surface of the working electrode was polished with alumina powder (0.05 μm) before each measurement and then washed by dimethylformamide to eliminate residual impurities. The auxiliary electrode was made of platinum wire, and the reference electrode was a silver wire pseudo-reference electrode. The calibration was done by measuring the formal potential of the ferrocenium/ferrocene (Fc^+/Fc) redox couple in DMF, which was found to be +0.07 V under the experimental conditions[24]. Cyclic voltammetric measurements were performed after switching on the automatic iR compensation function, so as to minimize the ohmic potential drop and to improve the accuracy of the potentials recorded. The total volume of DMF required for all samples was calculated according to the following equation:

$$\text{Total solvent volume} = \text{Volume required for one sample} \times \text{Number of samples} = 14 \times 7 = 98 \text{ mL}$$

Therefore, a total volume of 98 mL of DMF was required for the preparation and measurement of all investigated samples. The required mass of TBAP was calculated using the following equation:

$$\text{Mass of TBAP (g)} = \text{Conc. (mol L}^{-1}) \times \text{Molecular weight (g mol}^{-1}) \times \text{Volume (L)} 0.1 \times 341.91 \times \frac{98}{1000}$$

$$= 3.35 \text{ g}$$

Accordingly, 3.35 g of TBAP was dissolved in DMF to prepare the supporting electrolyte solution.

The required masses of the synthesized ligand and metal complexes were calculated according to the following equation: Mass (g) $= 10^{-3} \times 2 \times$ Molecular weight (g.mol^{-1}) $\times \frac{14}{1000}$

The concentrations of the ligand and complexes were adjusted to 2×10^{-3} mM, as summarized in **Table 5**.

Table 5. The mass of ligand and its metal complexes for cyclic voltammetry.

Comp. (2×10^{-3} mM)	L_1	CoL_1	NiL_1	CuL_1
Mass (g)	0.012	0.017	0.016	0.017

2.7. Cell culture and in vitro cytotoxicity assay

MCF-7 breast cancer cells and HBL-100 human mammary epithelial cells were used to conduct a preliminary *in vitro* cytotoxicity assessment of the free thiadiazole-based ligand (l1). The cells were obtained from the Iraq Biotech Cell Bank Unit in Basra. They were maintained in RPMI-1640 culture medium supplemented with 10% fetal bovine serum (FBS), 100 U/mL penicillin, and 100 µg/mL streptomycin. Cell subculturing was performed using Trypsin-EDTA solution, and the cells were incubated at 37°C in a humidified atmosphere containing 5% CO_2. HBL-100 cells were included as a non-tumorigenic human mammary epithelial cell model for comparison with the MCF-7 breast cancer cells.

For the cytotoxicity assay, cells were seeded in 96-well plates at a density of 1×10^4 cells/well and allowed to grow for 24 hours or until a confluent monolayer was formed prior to treatment. Subsequently, the cells were treated with compound l1 at concentrations of 15, 30, and 45 µg/mL, and cell viability was assessed 72 hours post-treatment.

Cell viability was determined using the MTT assay. Seventy-two hours after treatment, the culture medium was removed, and 28 µL of MTT solution (2 mg/mL) was added to each well, followed by a two-hour incubation at 37°C. Subsequently, the MTT solution was removed, and the formed formazan crystals were dissolved by adding 100 µL of dimethyl sulfoxide (DMSO), with incubation for 15 minutes at 37°C under agitation. Absorbance was measured at a wavelength of 620 nm using a microplate reader. The assay was performed in triplicate.

The proliferation rate (PR) was calculated using the equation: PR (%) = (B/A) × 100, where A represents the mean optical density of untreated cells and B represents the optical density of treated cells. The inhibition rate (IR) was calculated using the equation: IR (%) = 100 − PR (%).

3. Results and discussion

3.1. FT-IR spectra of ligands L_1 and metal complexes

The FT-IR spectrum of the ligand L_1 exhibited a broad band centered at 3147 cm^{-1} which was assigned to the N–H stretch[25]. Characteristic bands related to the CH=N and C=N stretching vibrations were observed at 1573 and 1600 cm^{-1}, respectively[26]. In addition, the symmetric stretching vibration of the C–S–C group appeared at 1205 cm^{-1}, while the skeletal vibration of the thiadiazole ring was detected at 1024 cm^{-1}. The spectra of the metal complexes exhibited noticeable shifts in the positions and intensities of the ligand bands, particularly those assigned to the C=N and CH=N groups, confirming their involvement in coordination with the metal ions[17]. Furthermore, new absorption bands attributed to the M–O and M–N stretching vibrations appeared at approximately 642 and 536 cm^{-1}, respectively, whereas the M–Cl stretching bands appeared within the 435–445 cm^{-1} region, consistent with the proposed coordination mode. The characteristic FT-IR spectral data are given in **Table 6** and **Figures 1 to 4**.

Table 6. FT-IR spectra of ligand L_1 and complexes.

Group	L_1	CoL_1	NiL_1	CuL_1
N-H	3147	3157	3142	3143
C-H (aromatic)	3007	3007	3007	3007
C-H (aliphatic)	2976	2976	2976	2976
C=N (Azo)	1602	1602	1602	1600
CH=N (endo)	1573	1575	1573	1573
C-SC (sy)	1163	1163	1163	1163
C-SC (asy)	1205	1205	1203	1205
Structural Movement	1024	1024	1024	1024
O-CH3 Ortho site-	2947	2947	2947	2945
O-CH3 Para site	2837	2837	2837	2837
C-O	1269	1267	1267	1267
M-N	---	536	536	586
M-Cl	---	435	445	437
M-O	---	642	642	642

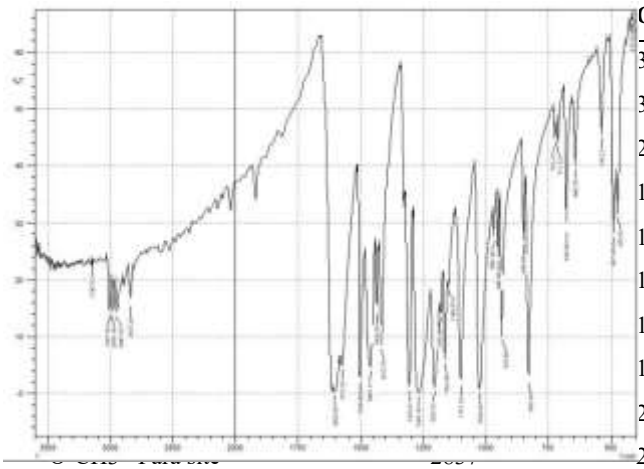


Figure 4. FT-IR spectrum of L_1.

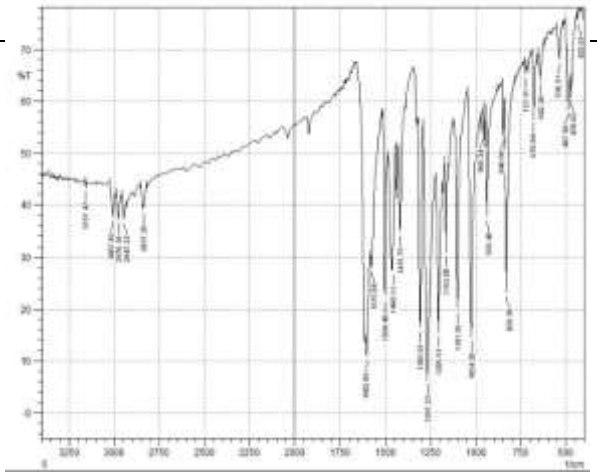


Figure 4. FT-IR spectrum of CoL_1.

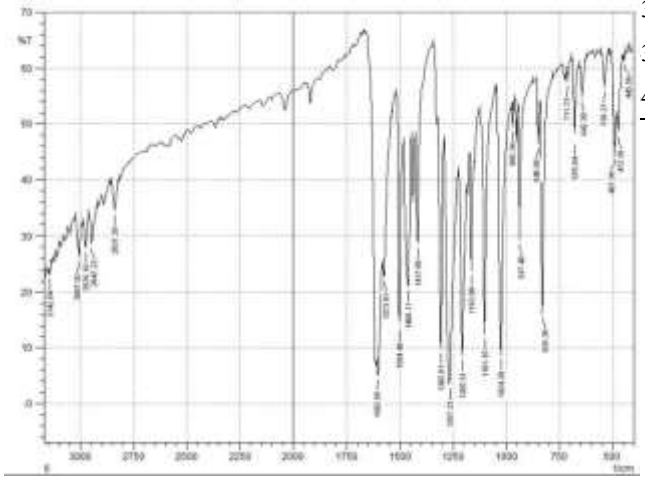


Figure 4. FT-IR spectrum of NiL_1.

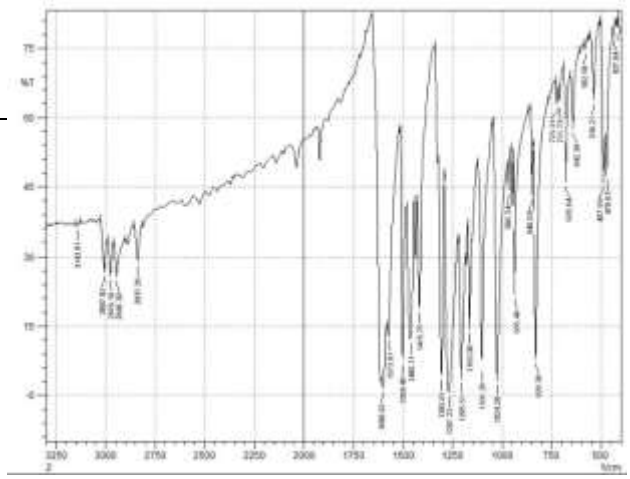


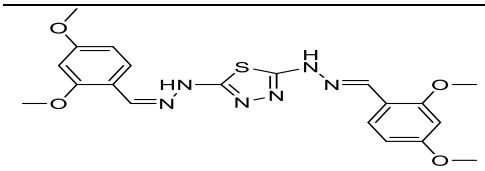
Figure 4. FT-IR spectrum of CuL_1.

3.2. ^{1}H and ^{13}C NMR spectra of ligand L_1

The proposed structure of ligand L_1 was confirmed by ^{1}H and ^{13}C NMR spectroscopy. In the ^{1}H NMR spectrum, a broad resonance at δ 10.19 ppm was assigned to the NH proton, with its broadening attributed to proton exchange[27]. The azomethine (CH=N) proton appeared as a characteristic signal at δ 8.82 ppm, which is consistent with the deshielding effect of the adjacent nitrogen atom and the conjugated electronic system. The aromatic protons resonated at δ 7.92–7.90 and 6.66–6.62 ppm, while the upfield shift of part of these signals was attributed to the electron-donating effect of the methoxy (OCH_3) substituents. In addition, two well-defined singlets observed at δ 3.89 and 3.84 ppm were assigned to the protons of the OCH_3 groups[28]. Their integrated intensities corresponded to approximately 12 protons, confirming the presence of four methoxy groups in agreement with the proposed molecular structure[29]. As shown in **Table 7** and **Figure 5**.

The chemical structure proposed was further confirmed by the ^{13}C NMR spectrum. A characteristic resonance for the azomethine carbon (C=N) was observed at δ 160.62 ppm[30], while the resonance observed at δ 155.97 ppm was attributed to the carbon that is bonded to the methoxy oxygen atom (Ar–C–OCH_3). The aromatic carbon resonances were observed at δ 128.19, 115.22, 107.05 and 98.75 ppm, whereas two other resonances at δ 56.36 and 56.00 ppm were assigned to carbon atoms of the OCH_3 groups[28]. The characteristic resonances in these spectra provide spectroscopic evidence for the presence of the methoxy substituents and corroborate the proposed structure of L_1. As shown in **Table 7** and **Figure 6**.

Table 7. ^{1}H and ^{13}C NMR spectra of ligand L_1.

Structural formulas	Type of NMR	NMR Data of (L_1)
	^{1}H-NMR	δ 10.19 (2H, br s, NH), 8.82 (2H, s, CH=N), 7.92–7.90 (2H, m, Ar-H), 6.66–6.62 (4H, m, Ar-H), 3.89, 3.84 (12H, s, OCH_3) ppm
	^{13}C-NMR	δ 160.62 (C=N), 155.97 (Ar–C–OCH_3), 128.19, 115.22, 107.05, 98.75 (Ar-C), 56.36, 56.00 (OCH_3) ppm

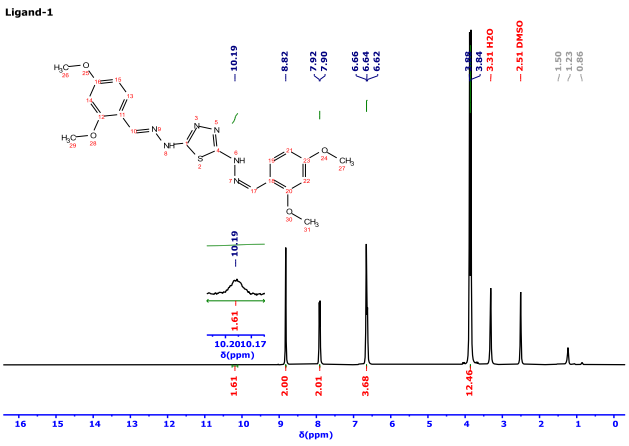


Figure 6. ^{1}H-NMR of L_1

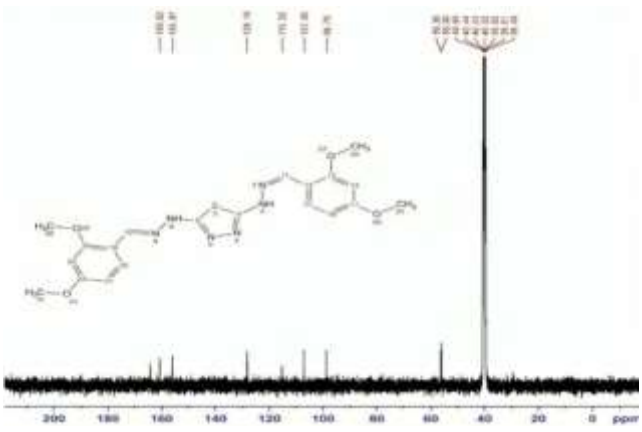


Figure 6. ^{13}C-NMR of L_1.

3.3. Mass spectra

The mass spectra of ligand L_1 and its metal complexes provided further evidence for the proposed molecular structures. The molecular ion (M^+) peaks were observed at m/z 442 for ligand L_1, m/z 608 for the Co(II) and Ni(II) complexes, and m/z 613 for the Cu(II) complex, in good agreement with their calculated molecular weights [31]. In all spectra, the same base peak was detected at m/z 149, corresponding to the fragment ion $[C_8H_9N_2O]^{\bullet}$, indicating that this structural fragment possesses high stability and is preferentially

formed during the fragmentation process [32]. The complete mass spectral data and the proposed fragmentation pathways of the synthesized compounds are presented in **Figures 7 to 10** and **Tables 8 to 11**.

Table 8. Mass fission of L_1 ligand.

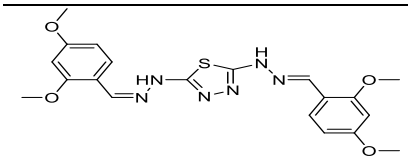
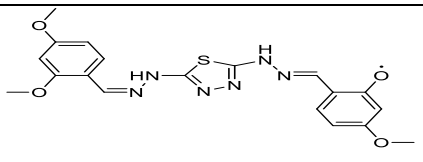
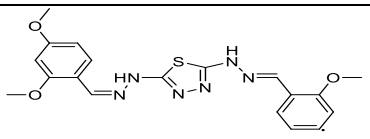
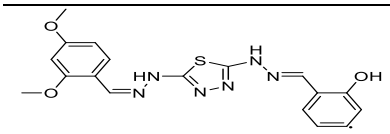
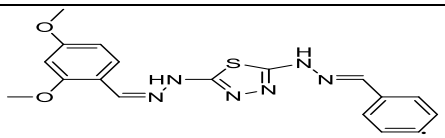
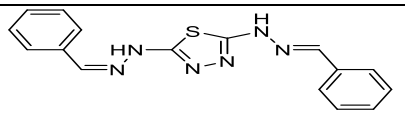
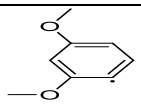
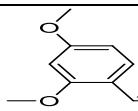
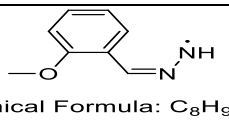
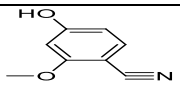
 Chemical Formula: $C_{20}H_{22}N_6O_4S$ Exact Mass: 442.1 Molecular Weight: 442.5	 Chemical Formula: $C_{19}H_{19}N_6O_4S^{\bullet}$ Exact Mass: 427.1 Molecular Weight: 427.5	 Chemical Formula: $C_{19}H_{19}N_6O_3S^{\bullet}$ Exact Mass: 411.1 Molecular Weight: 411.5
 Chemical Formula: $C_{18}H_{17}N_6O_3S^{\bullet}$ Exact Mass: 397.1 Molecular Weight: 397.4	 Chemical Formula: $C_{18}H_{17}N_6O_2S^{\bullet}$ Exact Mass: 381.1 Molecular Weight: 381.4	 Chemical Formula: $C_{16}H_{14}N_6S$ Exact Mass: 322.1 Molecular Weight: 322.4
 Chemical Formula: $C_8H_9O_2^{\bullet}$ Exact Mass: 137.1 Molecular Weight: 137.2	 Chemical Formula: $C_9H_{12}N_2O_2$ Exact Mass: 180.1 Molecular Weight: 180.2	 Chemical Formula: $C_8H_9N_2O^{\bullet}$ Exact Mass: 149.07 Molecular Weight: 149.17
 Chemical Formula: $C_8H_7NO_2$ Exact Mass: 149.0 Molecular Weight: 149.1		

Table *9.* Mass fission of CoL_1.

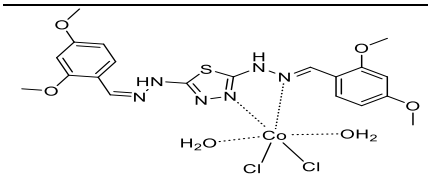
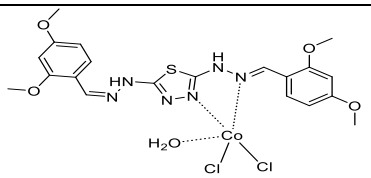
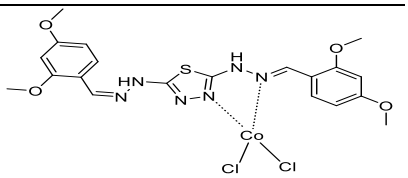
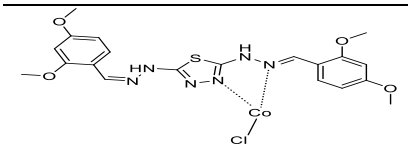
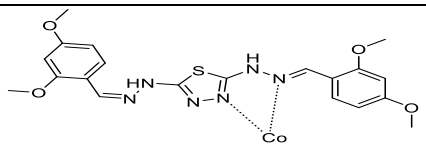
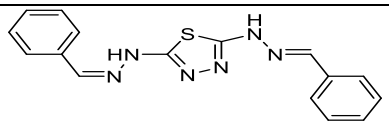
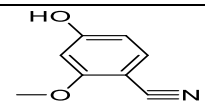
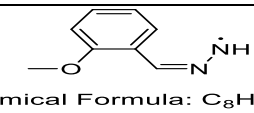
 Chemical Formula: $C_{20}H_{26}Cl_2CoN_6O_6S$ Exact Mass: 607.0 Molecular Weight: 608.4	 Chemical Formula: $C_{20}H_{24}Cl_2CoN_6O_5S$ Exact Mass: 589.0 Molecular Weight: 590.3	 Chemical Formula: $C_{20}H_{22}Cl_2CoN_6O_4S$ Exact Mass: 571.0 Molecular Weight: 572.3
 Chemical Formula: $C_{20}H_{22}ClCoN_6O_4S$ Exact Mass: 536.0 Molecular Weight: 536.9	 Chemical Formula: $C_{20}H_{22}CoN_6O_4S$ Exact Mass: 501.1 Molecular Weight: 501.4	 Chemical Formula: $C_{16}H_{14}N_6S$ Exact Mass: 322.1 Molecular Weight: 322.4
 Chemical Formula: $C_8H_7NO_2$ Exact Mass: 149.0 Molecular Weight: 149.1	 Chemical Formula: $C_8H_9N_2O^{\bullet}$ Exact Mass: 149.1 Molecular Weight: 149.2	

Table 10. Mass fission of NiL_1.

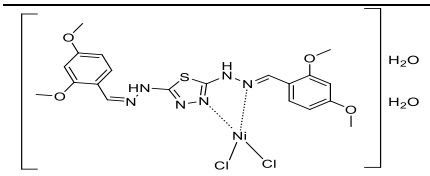
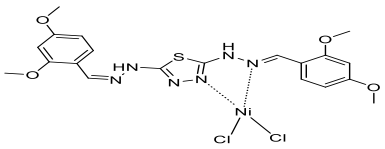
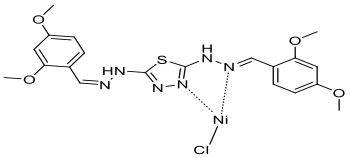
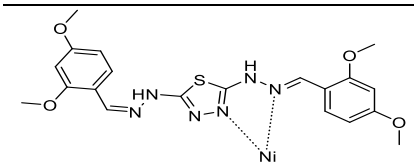
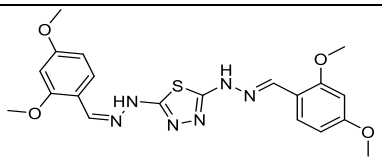
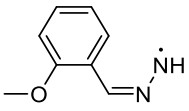
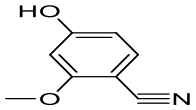
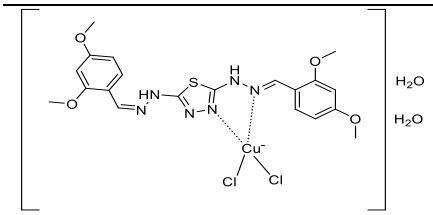
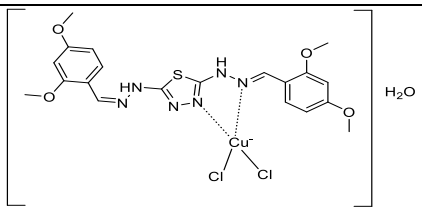
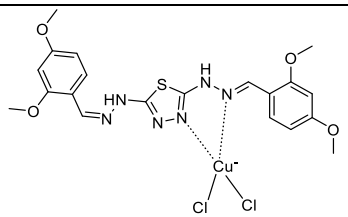
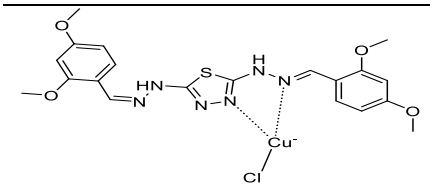
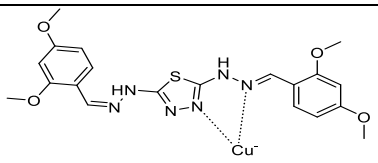
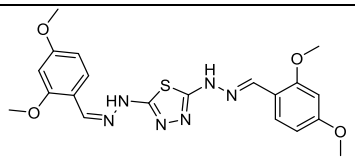
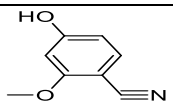
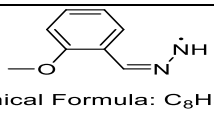
 Chemical Formula: $C_{20}H_{26}Cl_2N_6NiO_6S$ Exact Mass: 606 Molecular Weight: 608	 Chemical Formula: $C_{20}H_{22}Cl_2N_6NiO_4S$ Exact Mass: 570.0 Molecular Weight: 572.1	 Chemical Formula: $C_{20}H_{22}ClN_6NiO_4S$ Exact Mass: 535.0 Molecular Weight: 536.6
 Chemical Formula: $C_{20}H_{22}N_6NiO_4S$ Exact Mass: 500.1 Molecular Weight: 501.2	 Chemical Formula: $C_{20}H_{22}N_6O_4S$ Exact Mass: 442.1 Molecular Weight: 442.5	 Chemical Formula: $C_8H_9N_2O^{\bullet}$ Exact Mass: 149.1 Molecular Weight: 149.2
 Chemical Formula: $C_8H_7NO_2$ Exact Mass: 149.0 Molecular Weight: 149.1		

Table 11. Mass fission of CuL_1.

 Chemical Formula: $C_{20}H_{26}Cl_2CuN_6O_6S^-$ Exact Mass: 611 Molecular Weight: 613	 Chemical Formula: $C_{20}H_{24}Cl_2CuN_6O_5S^-$ Exact Mass: 593 Molecular Weight: 595	 Chemical Formula: $C_{20}H_{22}Cl_2CuN_6O_4S^-$ Exact Mass: 575.0 Molecular Weight: 576.9
 Chemical Formula: $C_{20}H_{22}ClCuN_6O_4S^-$ Exact Mass: 540.0 Molecular Weight: 541.5	 Chemical Formula: $C_{20}H_{22}CuN_6O_4S^-$ Exact Mass: 505.1 Molecular Weight: 506.0	 Chemical Formula: $C_{20}H_{22}N_6O_4S$ Exact Mass: 442.1 Molecular Weight: 442.5
 Chemical Formula: $C_8H_7NO_2$ Exact Mass: 149.0 Molecular Weight: 149.1	 Chemical Formula: $C_8H_9N_2O^{\bullet}$ Exact Mass: 149.1 Molecular Weight: 149.2	

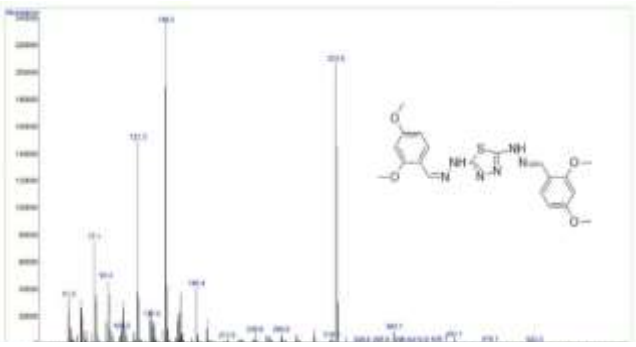


Figure 10. Mass spectrum of L_1.

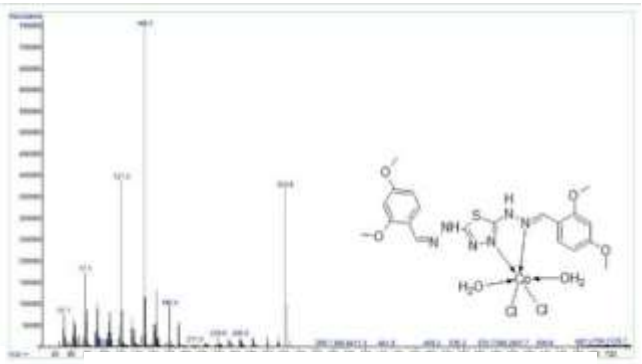


Figure 10. Mass spectrum of CoL_1.

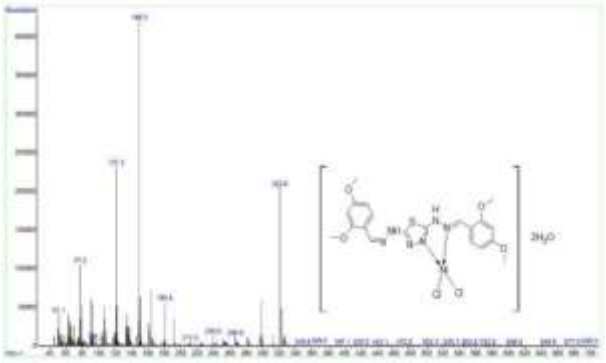


Figure 10. Mass spectrum of NiL_1.

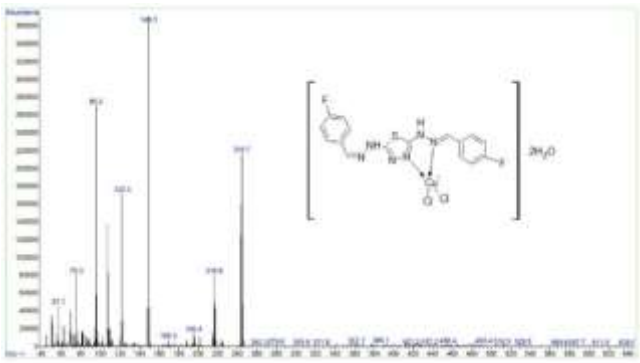


Figure 10. Mass spectrum of CuL_1.

3.4. UV–visible spectroscopy (UV–Vis)

The electronic absorption spectra of these synthesized ligands were obtained in DMF at 1×10^{-4} mol L^{-1} from 200–800 nm. The presence of several conjugated chromophoric units comprising the phenyl ring, azomethine (C=N) linkage, and thiadiazole ring resulted in the presence of characteristic π→π* and n→π* type of electronic transitions in the ligands. In general, the π→π* transitions were observed at shorter wavelengths, with relatively high absorption intensities, while the n→π* transitions were observed at longer wavelengths with relatively low intensities. The assignment of the absorption bands was based on the observed λmax values together with their absorption intensities and the structural features of the ligands[33]. Particular consideration was given to the extended π-conjugation and the presence of heteroatoms. The factors mentioned, particularly the presence of non-bonding electron pairs, may affect the electronic distribution and can give rise to overlapping or close absorption bands, notably corresponding to the azomethine group and the thiadiazole ring.

UV–Visible Spectra of Ligand L_1 and Its Metal Complexes :

Ligand L_1 exhibited four absorption bands at 280, 285, 291, and 421 nm, with molar absorptivity (ε) values of 5720, 5560, 5360, and 4870 $L \cdot mol^{-1} \cdot cm^{-1}$, respectively. The band centered at 421 nm was identified as the n→π* transition, while bands at 291, 285, and 280 nm were assigned to π→π* transitions of the azomethine group, the thiadiazole ring, and the phenyl ring, respectively[34]. The relatively large molar absorptivity values are consistent with the presence of allowed electronic transitions related to the extended π-conjugated system of the ligand. The π→π* transitions showed little change in wavelength, which indicates only electronic environment changes after complex formation when coordinated with Co(II), Ni(II), and Cu(II) ions, respectively. The n→π* band, however, showed a hypsochromic shift from 421 nm in the free ligand to 397, 395, and 401 nm for CoL_1, NiL_1, and CuL_1, respectively, which suggested the involvement of a nitrogen donor atom in coordination to the metal center[35]. Furthermore, a new band emerged at about 359 nm in all complexes, which was assigned to ligand-to-metal charge transfer (LMCT)[36]. The electronic spectra of the

complexes also showed weak absorption bands at 537, 729 and 744 nm for CoL_1, NiL_1 and CuL_1, respectively. These bands were attributed to d-d transitions, having a molar absorptivity of 1740, 370 and 2430 $L{\cdot}mol^{-1}{\cdot}cm^{-1}$, respectively[37]. The relatively low intensities of their bands are typical of Laporte-forbidden d–d transitions and agree with the suggested coordination geometry of the complexes synthesized[38]. As shown in **Table 12** and **Figures 11 to 14**.

Table 12. UV–visible spectra of ligand L_1 and its metal complexes.

Comp.	Λmax (nm)	Abs.	ε L.mol^{-1}.cm^{-1}	Transitions and assignment
L_1	421	0.487	4870	n→π*
	291	0.536	5360	π→π* (C=N) Azo
	285	0.556	5560	π→π*(C=N) 1,3,4-Thiadiazole ring
	280	0.572	5720	π→π* (C=C) Phenyl ring
CoL_1	537	0.174	1740	(d-d Transition)
	397	0.550	5500	n→π*
	359	0.640	6400	Charge Transfer(CT)
	300	0.348	3480	π→π* (C=N) Azo
	297	0.358	3580	π→π*(C=N) 1,3,4-Thiadiazole ring
	277	0.431	4310	π→π* (C=C) Phenyl ring
NiL_1	729	0.037	370	(d-d Transition)
	395	0.609	6090	n→π*
	359	1.008	10080	Charge Transfer(CT)
	294	0.630	6300	π→π* (C=N) Azo
	288	0.638	6380	π→π*(C=N) 1,3,4-Thiadiazole ring
	253	0.240	2400	π→π* (C=C) Phenyl ring
CuL_1	744	0.243	2430	(d-d Transition)
	401	0.588	5880	n→π*
	359	0.684	6840	Charge Transfer(CT)
	297	0.401	4010	π→π* (C=N) Azo
	289	0.431	4310	π→π*(C=N) 1,3,4-Thiadiazole ring
	277	0.474	4740	π→π* (C=C) Phenyl ring

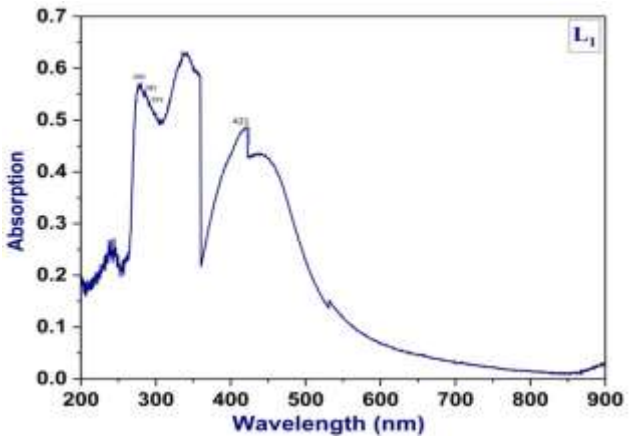


Figure 12. UV–visible spectrum of L_1.

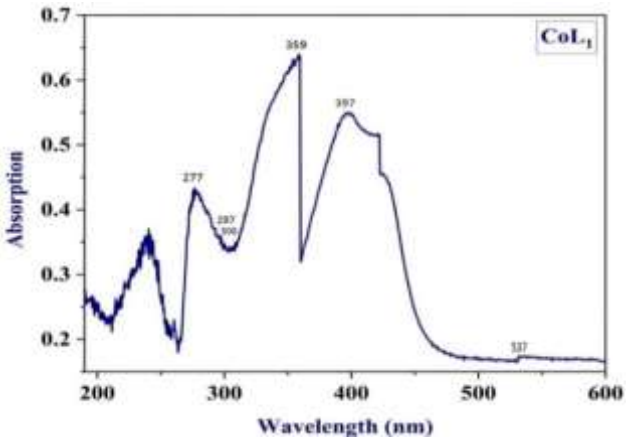


Figure 12. UV–visible spectrum of CoL_1.

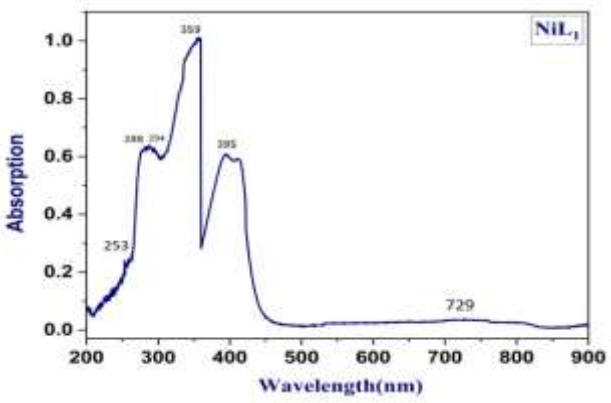


Figure 14. UV–visible spectrum of NiL_1.

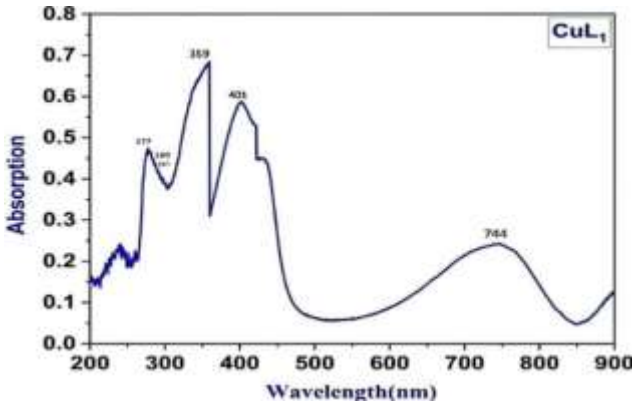


Figure 14. UV–visible spectrum of CuL_1.

3.5. molar conductivity

The molar conductivity data can also be useful in determining the ionic nature of coordination compounds and whether there are counter ions present in the outer sphere. The measured molar conductivity values showed that all the synthesized metal complexes are not electrolytes in solution, implying that there were no ions present in the outer sphere[39], as shown in **Table 13**.

The results were also confirmed through silver nitrate ($AgNO_3$) test results, where no white precipitate and no turbidity were seen after adding the reagent to the complex solutions. The overall conductivity and $AgNO_3$ test results are thus in accordance with the proposed molecular formulae and substantiate the non-electrolytic nature of the synthesized complexes[40].

Table 13. Molar electrical conductivity of the prepared complexes.

NO.	Complexes	Λm (s.cm^2.mole^{-1})	Electrolyte type
1	CoL_1	15.8	Non-electrolyte
2	NiL_1	11.1	Non-electrolyte
3	CuL_1	18.3	Non-electrolyte

3.6. Cyclic voltammetry (CV)

The electrochemical properties of this ligand (L_1), its respective Co(II), Ni(II), and Cu(II) complexes, as well as the precursor metal salts ($CoCl_2{\cdot}6H_2O$, $NiCl_2{\cdot}6H_2O$, and $CuCl_2{\cdot}6H_2O$), were explored using cyclic voltammetry (CV) in 0.1 M tetrabutylammonium perchlorate (TBAP)/DMF under an Ar atmosphere at room temperature. Electrochemical measurements were performed using a conventional single-compartment three-electrode cell consisting of a freshly polished 3 mm glassy carbon disk as the working electrode, a platinum wire as the counter electrode, and a silver pseudo-reference electrode. The reference electrode was calibrated against the Fc^+/Fc redox couple in DMF, giving a formal potential of +0.07 V under the employed experimental conditions, while iR compensation was automatically applied throughout the measurements[41]. Before each experiment, the working electrode was polished with 0.05 µm alumina paste, thoroughly rinsed with distilled water, and finally washed with DMF. All voltammograms were recorded at a scan rate of 100 mV s^{-1}, and all reported potentials are referenced to the silver pseudo-reference electrode[26,42]. The cyclic voltammograms of the ligands, their metal complexes, and the corresponding metal salts are presented in **Figures 15 to 17** and **Table 1.**

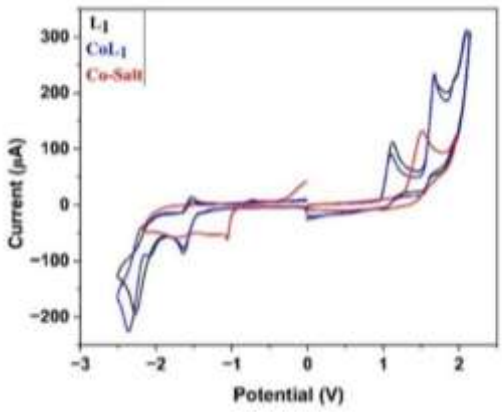


Figure 15. Cyclic voltammetry of L_1, CoL_1, $CoCl_2.6H_2O$

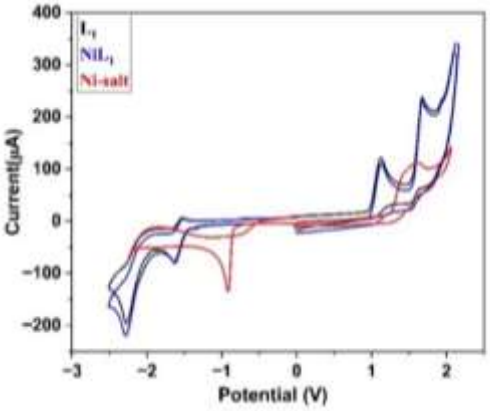


Figure 16. Cyclic voltammetry of L_1, NiL_1, $NiCl_2.6H_2O$.

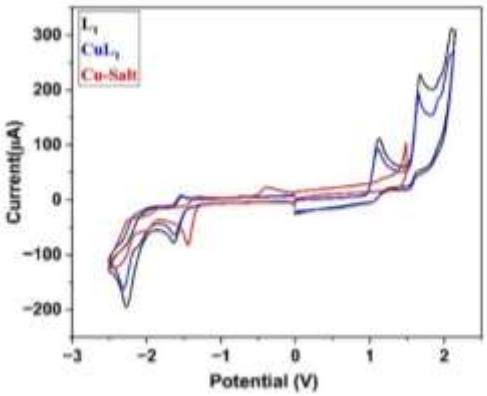


Figure 17. Cyclic voltammetry of L_1, CuL_1, $CuCl_2.6H_2O$.

Table 14. Cyclic voltammetry of ligand L_1, its metal complexes and salt.

compound	Concentration (mM)	Voltage Scan rate (V/S)	Ep_c (V)	ip_c (μA)	Ep_a (V)	ip_a (μA)	$E_{1/2}$ (V)	ΔEp (V)	ip_a/ip_c (μA)
L_1	2	0.1	≈-1.336 -1.636 -2.276 --- --- ≈1.551 ---	-5.565 -58.888 -73.019 --- --- 28.83 ---	--- ≈-1.534 --- -0.664 1.121 1.675 ≈1.92	--- -10.02 --- 2.807 103.751 168.307 40.561	--- -1.585 --- --- --- 1.613 ---	--- 0.102 --- --- --- 0.124 ---	--- 0.170 --- --- --- 5.733 ---
CoL_1	2	0.1	-1.641 -2.083 -2.365 --- --- --- ≈1.559 ---	-68.087 -15.557 -61.365 --- --- --- 27.036 ---	-1.534 --- --- ≈-2.217 -0.734 1.103 1.676 >1.92	14.105 --- --- -37.027 3.912 69.318 147.311 58.427	-1.587 --- --- --- --- --- 1.617 ---	0.107 --- --- --- --- --- 0.117 ---	-0.207 --- --- --- --- --- 5.448 ---

			-1.351	135.46	---	---	---	---	---
			-1.631	113.834	≈-1.542	150.574	-1.586	0.089	1.322
			-2.281	-73.555	---	---	---	---	---
NiL_1	2	0.1	---	---	1.13	90.478	---	---	---
			≈1.596	34.504	1.68	135.487	1.638	0.084	3.926
			---	---	>1.92	46.849	---	---	---
			-1.623	-67.151	-1.526	5.153	-1.574	0.097	-0.076
			>-2.098	-93.834	---	---	---	---	---
			-2.314	-165.879	---	---	---	---	---
			---	---	>-2.199	-63.616	---	---	---
CuL_1	2	0.1	---	---	-0.706	3.673	---	---	---
			---	---	1.108	74.253	---	---	---
			≈1.569	20.28	1.655	174.055	1.612	0.086	8.582
			---	---	≈1.873	176.041	---	---	---
			-1.06	-11.907	---	---	---	---	---
			-1.205	-4.01	-1.221	51.16	-1.213	-0.016	12.758
			<-1.213	-3.734	---	---	---	---	---
$CoCl_2.6H_2O$	3	0.1	-1.718	-8.963	---	---	---	---	---
			---	---	1.51	116.943	---	---	---
			≈1.032	-6.019	---	---	---	---	---
			-0.913	-111.805	---	---	---	---	---
$NiCl_2.6H_2O$	3	0.1	---	---	≈-2.173	-28.843	---	---	---
			---	---	1.627	99.833	---	---	---
			-0.301	-6.204	---	---	---	---	---
			-0.510	-2.923	---	---	---	---	---
			<-1.55	3.382	---	---	---	---	---
$CuCl_2.6H_2O$	3	0.1	≈-2.15	-21.814	---	---	---	---	---
			---	---	-0.39	61.601	---	---	---
			---	---	≈1.15	17.956	---	---	---

"---" indicates that no corresponding anodic or cathodic peak was observed for the respective redox process; therefore, the related electrochemical parameters could not be determined.

The first reduction process of the free L_1 (E_{pc}^1 =-1.636 V) was anodically shifted and noted at -1.631 V and -1.623 V after complexation with Ni^{2+} and Cu^{2+} ions, respectively; see **Figures 17 and 18**. These anodic shifts for the complexed L_1 agree well with the decrease in electron density for the complexed ligand, which leads to reduced reduction ease. The easier first reduction was noted in CuL_1 (-1.623 V) compared to NiL_1 (-1.631 V). In the case of CoL_1, a harder first reduction process was noted at -1.641 V compared with that (-1.636 V) of the free ligand L_1. This cathodic shift is consistent with possible back-bonding in the CoL_1 complex [43]. The second cathodic peak potentials (E_{pc}^1) for the complexed L_1 in CoL_1, NiL_1 and CuL_1 were cathodically shifted compared with that of the free ligand (E_{pc}^2 =-2.276 V). They occurred respectively at -2.365 V, -2.281 V and -2.314 V. These difficult second reductions for complexed L_1 correspond to the stability of the complexed $L_1^{\cdot-}$ This $L_1^{\cdot-}$ Stability and hence the increase in difficulty of the second reduction follow the order: $NiL_1 < CuL_1 < CoL_1$. Interesting weak reduction waves are noted in CoL_1 and CuL_1 at -2.083 V and >-2.098 V, respectively. These reductions are assigned to the whole complex systems themselves. The irreversible weak oxidation process of the free ligand noted at -0.664 V is cathodically shifted in CoL_1 (-0.734 V) and CuL_1 (-0.706 V), which refers to the difficulty of this oxidation after complexation. Like the free ligand L_1, its complexes showed two main oxidation processes and a third weak oxidation process. The first oxidation

process in CoL_1 and CuL_1 is easily compared with that of the free L_1 (1.121 V), noted respectively at 1.103 V and 1.108 V. This cathodic shift is attributed to the possible back-bonding in these two complexes. The absence of back-bonding in NiL_1 renders the complexed L_1 to be oxidized at a harder potential (1.13 V) compared with that of the free L_1. As noted before for ligands and L_1 complexes, the second oxidation occurs at a more positive potential in L1 complexes than in free L1, which is attributed to the stability of the complexed $L_1^{+\cdot}$ (formed after the first oxidation).

The cyclic voltammograms (CVs) of the precursor metal salts were recorded and are presented in **Figures 15, 16, and 17**, while the corresponding oxidation and reduction peak potentials are summarized in **Table 14**. No distinct metal-centered redox processes were observed for the synthesized complexes, indicating that the recorded electrochemical responses are predominantly associated with ligand-centered electron-transfer processes.

The first cathodic peak potential (Epc_1) provides insight into the electron density of the coordinated ligand. A less negative Epc_1 value corresponds to a more favorable reduction process and therefore reflects a lower electron density around the ligand framework. Based on the Epc_1 values, the electron density of the complexes increased in the following order: $CuL_1 < NiL_1 < CoL_1$. The second cathodic peak potential (Epc_2) was used to evaluate the stability of the reduced radical species ($L_n^{-}\bullet$) generated after the first reduction step. More negative Epc_2 values indicate more stabilization of the reduced intermediate. Accordingly, the stability of the reduced species increased in the order: $NiL_1 < CuL_1 < CoL_1$.

In conclusion, the electrochemical study showed significant differences between the free ligand and its metal complexes. The appearance, disappearance, and displacement of the redox waves are indicative of changes in the electronic environment as a result of Ligand coordination, and evidence for variations in electron density, complex stability, electron delocalization, and the possibility of metal-to-ligand back-donation interactions[44].

3.7. Computational analysis of the electron density distribution

The Gaussian package was used for the computational calculations, while GaussView 6.0 was used for constructing and visualizing the molecular structures. Electron density calculations were performed on the prepared ligand to study the electron density distribution and identify the most probable coordination sites. The proposed metal complexes were constructed and visualized using GaussView 6.0 based on experimental spectral data and the coordination behavior of the ligands. No quantum chemical calculations were performed on the metal complexes[45].

The calculated electron density distribution of compound L_1 was used to identify the most probable coordination sites. Subsequently, metal complexes were constructed as proposed coordination models using GaussView 6.0 software, based on experimental spectroscopic and electrochemical data. No quantum-chemical optimization was performed on these metal complexes. Based on experimental spectroscopic data and proposed coordination models, the tetrahedral geometric structure of the Ni(II) and Cu(II) complexes was determined, while the octahedral geometric structure of the Co(II) complex was proposed[46]. As shown in **Figures 18 to 22**.

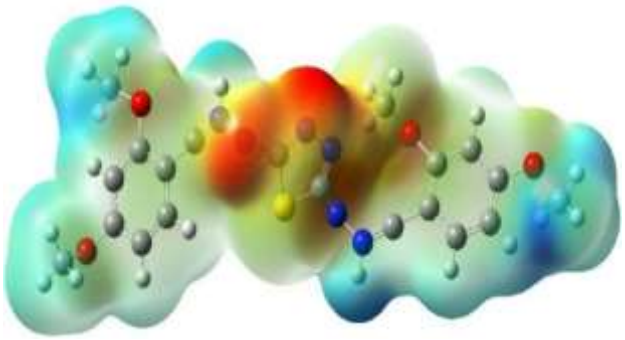


Figure 21. L_1 of EMP.



Figure 21. Molecular Structure of L_1.

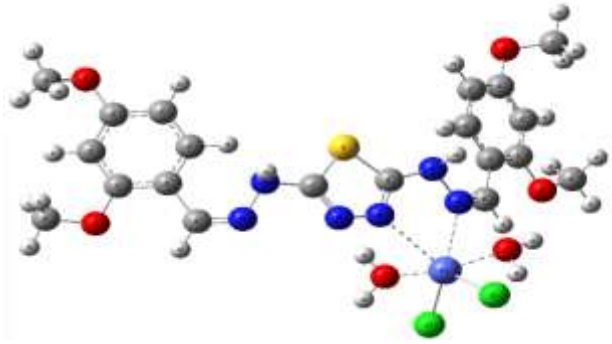


Figure 21. Proposed structure of CoL_1 constructed using GaussView 6.0.

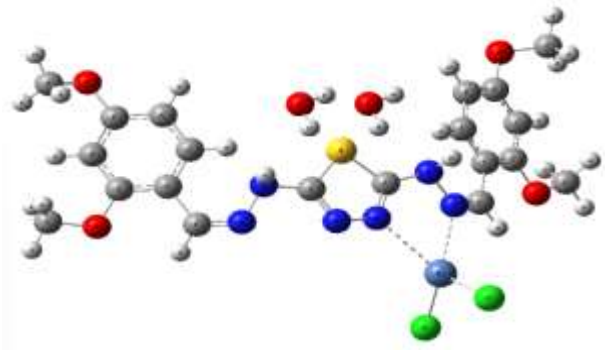


Figure 21. Proposed structure of NiL_1 constructed using GaussView 6.0.

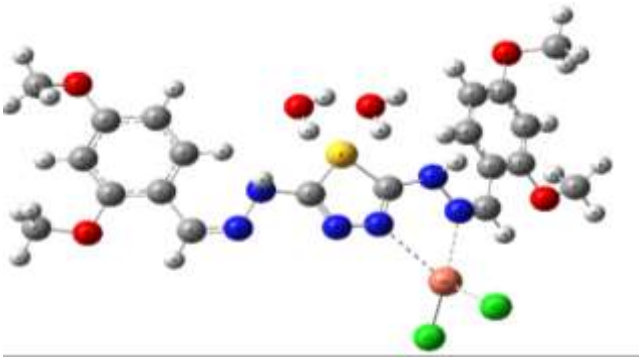


Figure 21. Proposed structure of CuL_1 constructed using gaussview 6.0.

3.8. Preliminary in vitro cytotoxicity of L1 against MCF-7 and HBL-100 cells

The synthesized ligand was tested for its in vitro anticancer activity against MCF-7 cells, commonly used as an in vitro model in breast cancer research. The non-tumorigenic human breast epithelial cell line, HBL-100, a non-tumorigenic human mammary epithelial cell line, were included as a comparative model. Both cell lines were used so that the compound's effect on the growth of cancer cells could be compared with its toxicity to normal cells[47].

The preliminary in vitro cytotoxicity of the free thiadiazole ligand (L1) was evaluated against MCF-7 breast cancer cells and HBL-100 human mammary epithelial cells at concentrations of 15, 30, and 45 µg/mL. As shown in Figure 23, the growth inhibition rates for MCF-7 cells were 2.32%, 13.11%, and 6.85% at concentrations of 15, 30, and 45 µg/mL, respectively; consequently, the highest inhibition rate for MCF-7 cells was observed at a concentration of 30 µg/mL (13.11%). In contrast, the inhibition rates for HBL-100 cells were 4.88%, 4.51%, and 6.77% at concentrations of 15, 30, and 45 µg/mL, respectively, remaining relatively low across the tested concentration range. Since the inhibition rate for MCF-7 cells did not reach 50% at any of the tested concentrations, it was not possible to determine the half-maximal inhibitory concentration (IC_{50}) value under the experimental conditions employed.[48]. These results indicate that additional testing at higher concentrations is necessary to establish if increasing growth inhibition can be achieved. Further, comparison of L_1 with other cancer cell lines could help explain its biological activity since the cellular response might differ between tumor types[12]. The inhibition results are presented in **Figure 23**.

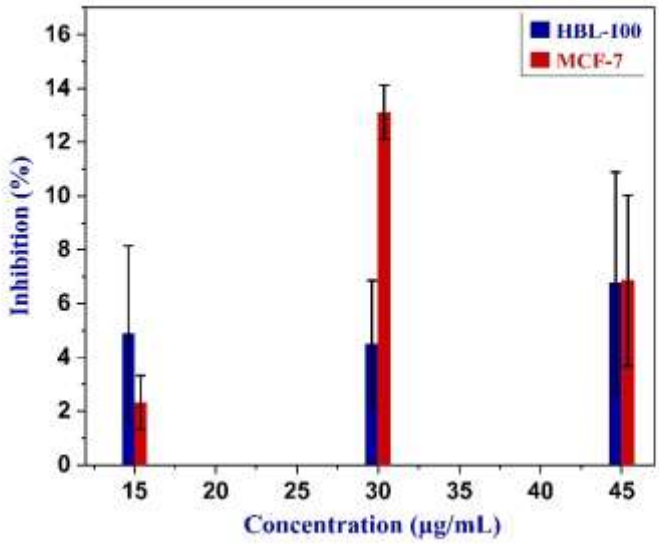


Figure 23. Percentage inhibition of MCF-7 and HBL-100 cells by L1 at different concentrations. Data are presented as the mean ± SD of triplicate measurements

4. Conclusions

A thiadiazole-based ligand (L_1) and its complexes with Co(II), Ni(II), and Cu(II) ions were prepared and characterized using FT-IR, UV-Visible, $^1H/^{13}C$ NMR, and mass spectrometry, as well as molar conductivity measurements. Conductivity measurements and silver nitrate ($AgNO_3$) tests confirmed the non-electrolytic nature of the prepared complexes. Cyclic voltammetry revealed that coordination with the metal altered the redox behavior of ligand L_1, although no distinct metal-centered redox couple was clearly observed under the experimental conditions employed. Electron density calculations were performed for ligand L_1, while the structures of the metal complexes were constructed as proposed coordination models based on experimental data; no quantum-chemical optimization of the metal complex structures was conducted. Based on the

experimental spectroscopic data and proposed structural models, a tetrahedral geometry was assigned to the Ni(II) and Cu (II) complexes, whereas an octahedral geometry was proposed for the Co(II) complex. Additionally, a preliminary cytotoxicity assessment of the free ligand L_1 alone was conducted against MCF-7 and HBL-100 cell lines. Ligand L_1 did not achieve 50% inhibition at concentrations of 15, 30, or 45 µg/mL; consequently, an IC_{50} value could not be determined under these test conditions. As no biological evaluation of the metal complexes was performed, no conclusions can be drawn regarding the enhancement of anticancer activity resulting from metal coordination.

Conflict of interest

The author declares no conflict of interest.

Acknowledgements

Professors of the Chemistry Department, College of Science, University of Thi Qar, Iraq

Declaration of generative AI in scientific writing

Some artificial intelligence tools were used in text rewriting and grammatical language improvement.

CRediT author statement

Zainab Majed Kareem: Supervision.

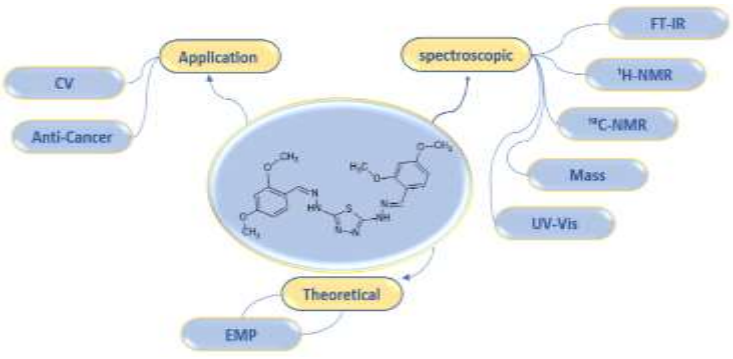
Noor Lateef Kadim: Writing - Reviewing and Editing.

Highlights

- A new thiadiazole-based ligand (L_1) and its Co(II), Ni(II), and Cu(II) complexes were synthesized and characterized by FT-IR, UV–Vis, $^1H/^{13}C$ NMR, mass spectrometry, and molar conductivity.
- Molar conductivity confirmed that all complexes are non-electrolytic, supporting the proposed coordination geometry with no counterions outside the coordination sphere.
- Cyclic voltammetry revealed ligand-centered (not metal-centered) redox behavior, with electron density and reduced-species stability trends established across the CoL_1, NiL_1, and CuL_1 complexes.
- Electron density calculations were performed for compound L1, while the structures of the metal complexes were constructed as proposed coordination models using the GaussView 6.0 software.
- A preliminary in vitro cytotoxicity assay was conducted for the free ligand L1 against MCF-7 and HBL-100 cells.

Novelty: This is the first study to integrate spectroscopic and electrochemical (cyclic voltammetry) data for a single thiadiazole ligand system across Co(II), Ni(II), and Cu(II) complexes under identical conditions, a combination not previously addressed in the literature. Furthermore, the study includes a preliminary cytotoxicity assessment against MCF-7 breast cancer cells and HBL-100 human mammary epithelial cells.

Graphical abstract



References

1. Daoud, A.M.: 'Synthesis, characterization and evaluation biological activity of new Schiff base compounds and their complexes with some transition elements', University of Thi-Qar Journal of Science, 2017, 6, (2), pp. 81-90.
2. Katea, A.H.: 'Synthesis, Characterization, Antimicrobial New 2, 2'-[(1E, 2E)-ethane-1, 2-diylidenedi (2E) hydrazin-1-yl-2-ylidene] bis (5-methyl-1, 3, 4-oxadiazole) and their transition metal complexes', University of Thi-Qar Journal of Science, 2017, 6, (2), pp. 1-18.
3. Alkafiji, N.A.A.: 'Preparation, Characterization and Biological Study of New Derivatives of 1, 3, 4-Thiadiazoleand Its Complexes with Some Transitional Element Ions', University of Thi-Qar Journal of Science, 2017, 6, (3), pp. 90-100.
4. Jain, A.K., Sharma, S., Vaidya, A., Ravichandran, V., and Agrawal, R.K.: '1, 3, 4-Thiadiazole and its derivatives: A review on recent progress in biological activities', Chemical biology & drug design, 2013, 81, (5), pp. 557-576.
5. Hu, Y., Li, C.-Y., Wang, X.-M., Yang, Y.-H., and Zhu, H.-L.: '1, 3, 4-Thiadiazole: synthesis, reactions, and applications in medicinal, agricultural, and materials chemistry', Chemical reviews, 2014, 114, (10), pp. 5572-5610.
6. Li, Y., Geng, J., Liu, Y., Yu, S., and Zhao, G.: 'Thiadiazole—A promising structure in medicinal chemistry', ChemMedChem, 2013, 8, (1), pp. 27-41.
7. Indelicato, S., Bongiorno, D., Mauro, M., and Cascioferro, S.: 'Recent developments of 1, 3, 4-thiadiazole compounds as anticancer agents', Pharmaceuticals, 2025, 18, (4), pp. 580.
8. Daravath, S., Kumar, M.P., Rambabu, A., Vamsikrishna, N., and Ganji, N.: 'Design, synthesis, spectral characterization, DNA interaction and biological activity studies of copper (II), cobalt (II) and nickel (II) complexes of 6-amino benzothiazole derivatives', Journal of Molecular Structure, 2017, 1144, pp. 147-158.
9. Kuate, M., Conde, M.A., Ngandung Mainsah, E., Paboudam, A.G., Tchieno, F.M.M., Ketchemen, K.I., Tonle Kenfack, I., and Ndifon, P.T.: 'Synthesis, Characterization, Cyclic Voltammetry, and Biological Studies of Co (II), Ni (II), and Cu (II) Complexes of a Tridentate Schiff Base, 1-((E)-(2-Mercaptophenylimino) Methyl) Naphthalen-2-ol (H2L1)', Journal of Chemistry, 2020, 2020, (1), pp. 5238501.
10. Venkatesh, G., Vennila, P., Kaya, S., Ahmed, S.B., Sumathi, P., Siva, V., Rajendran, P., and Kamal, C.: 'Synthesis and spectroscopic characterization of Schiff base metal complexes, biological activity, and molecular docking studies', ACS omega, 2024, 9, (7), pp. 8123.
11. Obakachi, V.A., Kushwaha, B., Kushwaha, N.D., Mokoena, S., Ganai, A.M., Pathan, T.K., van Zyl, W.E., and Karpoormath, R.: 'Synthetic and anti-cancer activity aspects of 1, 3, 4-thiadiazole containing bioactive molecules: A concise review', Journal of Sulfur Chemistry, 2021, 42, (6), pp. 670-691.
12. Janowska, S., Khylyuk, D., Bielawska, A., Szymanowska, A., Gornowicz, A., Bielawski, K., Noworól, J., Mandziuk, S., and Wujec, M.: 'New 1, 3, 4-thiadiazole derivatives with anticancer activity', Molecules, 2022, 27, (6), pp. 1814.
13. Sayiner, H.S., Yilmazer, M.I., Abdelsalam, A.T., Ganim, M.A., Baloglu, C., Altunoglu, Y.C., Gür, M., Saracoglu, M., Attia, M.S., and Mahmoud, S.A.: 'Synthesis and characterization of new 1, 3, 4-thiadiazole derivatives: study of their antibacterial activity and CT-DNA binding', RSC advances, 2022, 12, (46), pp. 29627-29639.
14. TORAMBETOV, B., and KADİROVA, S.: 'RECENT ADVANCES IN 1, 3, 4-THIADIAZOLE-BASED METAL COMPLEXES: COORDINATION CHEMISTRY, CRYSTAL STRUCTURES, AND BIOLOGICAL ACTIVITIES', An overview of Coordination Chemistry with Metals, Ligands, Complexes and Applications: In Honor of Hacali Necefoğlu's 70th Birthday, 2025, pp. 101.
15. Soleiman-Beigi, M., Alikarami, M., Kohzadi, H., and Akbari, Z.: 'Dipotassium 1, 3, 4-thiadiazole-2, 5-bis (thiolate) as a new S-donor for direct synthesis of symmetrical disulfides', Scientific Reports, 2022, 12, (1), pp. 16149.
16. Kumar, D., Aggarwal, N., Kumar, V., Chopra, H., Marwaha, R.K., and Sharma, R.: 'Emerging synthetic strategies and pharmacological insights of 1, 3, 4-thiadiazole derivatives: a comprehensive review', Future Medicinal Chemistry, 2024, 16, (6), pp. 563-581.
17. Alsanafi, A.M., and Flifel, I.A.: 'Syntheses, Characterization of a New Legend 2-Hydroxy-N'-(5-Phenyl-1, 3, 4-Oxadiazol-2-yl) Benzohydrazide with Some Transition Metal Complexes', Annals of the Romanian Society for Cell Biology, 2021, 25, (6).
18. Herbert, C.A., and Jarvo, E.R.: 'Nickel-catalyzed stereoselective coupling reactions of benzylic and alkyl alcohol derivatives', Accounts of Chemical Research, 2023, 56, (22), pp. 3313.
19. Badade, S.S., Pansare, D.N., Shelke, R.N., Kashid, P., and Bembalkar, S.R.: 'Synthesis and Antimicrobial Screening of Metal-ligand Complexes Derivative from (2-chloroquinolin-3-yl) methylene) hydrazine) and their Biological Studies', Oriental Journal of Chemistry, 2025, 41, (3).
20. Yue, L., Debije, M.G., and Schenning, A.P.: 'Stimuli-responsive afterglow from luminescent liquid crystal elastomers', Advanced Materials, 2026, 38, (7), pp. e16922.
21. Kyhoiesh, H.A.K., and Al-Adilee, K.J.: 'Synthesis, spectral characterization and biological activities of Ag (I), Pt (IV) and Au (III) complexes with novel azo dye ligand (N, N, O) derived from 2-amino-6-methoxy benzothiazole', Chemical Papers, 2022, 76, (5), pp. 2777-2810.

22. Ahmed, Y.M., Ashmawy, A.M., Omar, M., Abbas, A.A., Mostafa, S.G., and Mohamed, G.G.: 'Synthesis, characterization, biological activity, DFT studies on transition metal complexes derived from 5, 5′-(propane-1, 3-diylbis (sulfanediyl)) bis (1, 3, 4-thiadiazol-2-amine) ligand and its corrosion inhibition study on carbon steel', Journal of Molecular Structure, 2023, 1280, pp. 134956.
23. Gatea, A.H., Abdul-Hassan, W.S., Ali, S., and Mahdi, Z.: 'Ligand Adducts of Bis (acetylacetonato) Copper (II), Bis (3-chloroacetylacetonato) Copper (II) with 4, 4'-bipyridine, and Propylene Spacered Bis-viologen', Journal of Medicinal and Chemical Sciences, 2023, 6, (2), pp. 280-303.
24. Gatea, A.H., and Alshamkhawy, S.A.A.: 'Comparison Study of Cloud Point and Solvent Extraction of Copper by 3-Chloro-2, 4-pentanedione as Complexing Agent', 2022.
25. A. Majed, A., Al-Duhaidahawi, D., A. Omran, H., Abbas, S., S. Abid, D., and Y. Hmood, A.: 'Synthesis, molecular docking of new amide thiazolidine derived from isoniazid and studying their biological activity against cancer cells', Journal of Biomolecular Structure and Dynamics, 2024, 42, (24), pp. 13485-13496.
26. Alsanafi, A.M., and Al-Saadawy, N.H.: 'Synthesis, Characterization, Cyclic Voltammetry (CV), Theoretical Molecular Docking against Breast Cancer and Computational Study to Determine the Energy Gap of a Newly Series of Organotillium Compounds Based on N-(4-Benzoylphenyl)–2–Tellerocyanatoacetamide', Trends in Sciences, 2025, 22, (9), pp. 10416-10416.
27. Lin, W.-D., Lee, Y.-C., Cheng, H.-C., Lo, H.-H., Mehmood, A., Yang, C.-N., and Lu, P.-J.: 'Structural and functional characterization of Pin1BP1: A novel Pin1-interacting protein regulating apoptosis', International Journal of Biological Macromolecules, 2025, 319, pp. 145587.
28. Mahdi, H.F.A., and Al-Lami, N.: 'Synthesis, Spectral Characterization, and Multi-Scale Computational Insights Into Imidazo [1, 2-a] pyridine–Thiadiazole-Based Schiff Bases', ChemistrySelect, 2026, 11, (24), pp. e73711.
29. OSHITA, A., Takegoshi, M., Kato, M., Okamoto, C., and Kato, S.: 'Polyurethane for polishing layer, polishing layer including polyurethane and modification method of the polishing layer, polishing pad, and polishing method', in Editor (Ed.)^(Eds.): 'Book Polyurethane for polishing layer, polishing layer including polyurethane and modification method of the polishing layer, polishing pad, and polishing method' (Google Patents, 2021, edn.), pp.
30. Radha, V.P., and Prabakaran, M.: 'Novel thiadiazole-derived Schiff base ligand and its transition metal complexes: Thermal behaviour, theoretical study, chemo-sensor, antimicrobial, antidiabetic and anticancer activity', Applied Organometallic Chemistry, 2022, 36, (11), pp. e6872.
31. Sallam, M., Metwaly, A.M., and Ragab, E.A.E.-W.: 'UPLC-Triple TOF-MS/MS Phytochemical Profiling and In Vitro Evaluation of Saraca cauliflora Bak. Methanolic Leaf Extract', Egyptian Journal of Chemistry, 2025.
32. Abdulrazzaq, A.G., Abood, S.S., and Al-Hamdani, A.A.S.: 'Synthesis, characterization, thermal analysis and antioxidant determination for some metal ions complexes with new ligand', Bulletin of the Chemical Society of Ethiopia, 2025, 39, (11), pp. 2129-2144.
33. Ejiah, F.N., Rofiu, M.O., Oloba-Whenu, O.A., and Fasina, T.M.: 'Schiff bases as analytical tools: synthesis, chemo-sensor, and computational studies of 2-aminophenol Schiff bases', Materials Advances, 2023, 4, (10), pp. 2308-2321.
34. Venkatesh, R., Murugan, T., Kubaib, A., Umamaheswari, L., Imran, P.M., AbdelGawwad, M.R., Alayadi, H., and Alfrisany, N.M.: 'Exploring the chemical and biological landscape of a Nickel (II) schiff base complex via azomethine linkage', Scientific Reports, 2025, 16, (1), pp. 2256.
35. Es-Sounni, B., Nakkabi, A., Bouymajane, A., Elaaraj, I., Bakhouch, M., Filali, F.R., El Yazidi, M., El Moualij, N., and Fahim, M.: 'Synthesis, characterization, antioxidant and antibacterial activities of six metal complexes based tetradentate salen type bis-Schiff base', Biointerface Res. Appl. Chem, 2023, 13, (4), pp. 333.
36. Nguyen, Q.T., Pham Thi, P.N., and Nguyen, V.T.: 'Synthesis, characterization, and in vitro cytotoxicity of unsymmetrical tetradentate Schiff base Cu (II) and Fe (III) complexes', Bioinorganic chemistry and applications, 2021, 2021, (1), pp. 6696344.
37. Borghesani, V., Zastrow, M.L., Tolbert, A.E., Deb, A., Penner-Hahn, J.E., and Pecoraro, V.L.: 'Co (II) substitution enhances the esterase activity of a de novo designed Zn (II) carbonic anhydrase', Chemistry–A European Journal, 2024, 30, (24), pp. e202304367.
38. Arifin, H.W.M., Mohd, W., Ali, N.M., Bakar, N.A., Mustafar, S., Ahmad, M.S., Taha, H., Supian, F.L., and Osman, U.M.: 'A selective fluorescent chemosensor based on chromone hydrazone ligand for Zinc ions', Central Asia & the Caucasus (14046091), 2022, 23, (1), pp. 2011.
39. Kumar, B.R.C., Babu, K.S., and Shabana, P.: 'SYNTHESIS, CHARACTERIZATION, AND BIOLOGICAL EVALUATION OF NOVEL HETEROCYCLIC PYRIDINE BASED THIOPHENE DERIVATIVE OF TRANSITION METAL COMPLEXES', European Journal of Biomedical, 2022, 9, (1), pp. 278-288.
40. Husenov, K.S., Umarov, B.B., Turgunov, K.K., Sharipov, S.S., Ganiev, B.S., Akhtamov, D.T., and Safin, D.A.: 'Synthesis, characterization and computational studies of the triangle shape complex of silver nitrate with 2-amino-1, 3, 4-thiadiazole', Polyhedron, 2025, 267, pp. 117259.
41. Al-Taher, A.H., Mejbel, H.K., Al-Badry, L.F., and Abdul-Hassan, W.S.: 'Influence of end groups (4F, 4Br, 4CF3, and 4CBr3) of non-fullerene acceptor molecules on the performance of organic solar cells', Journal of Nanoparticle Research, 2025, 27, (4), pp. 96.

42. Alibrahimi, A.A., and Abdul-Hassan, W.S.: ‘Design and Synthesis of Novel Molecular Switches Functionalized with a Viologen Unit Based on Copper (II) Bis (ethyl 4-chloroacetoacetate) Complex’, EURASIAN JOURNAL OF CHEMISTRY, 2026, 31, (2 (122)), pp. 16-40.
43. Muhamed, M.A., and Abdul, H.W.S.: ‘Iron (II), cobalt (II), and nickel (II) complexes of bis-(3-chloroacetylacetonate) ethylenediimine and bis-(acetylacetonate) ethylenediimine and their viologen molecular switches’, 2023.
44. Alibrahimi, A.A., and Abdul-Hassan, W.S.: ‘Molecular Switches Incorporating the Adducts Among Viologen unints and both Copper Bis (ethylacetoacetate) and Copper Bis (ethyl 4-chloroacetoacetate)’, Vascular and Endovascular Review, 2025, 8, (6s), pp. 151-182.
45. Kabilan, S.J., Sivakumar, O., Kunjiappan, S., Pavadai, P., and Sundar, K.: ‘Molecular modelling approaches for the identification of potent sodium-glucose cotransporter 2 inhibitors from Boerhavia diffusa for the potential treatment of chronic kidney disease’, Journal of Research in Pharmacy, 2025, 29, (5), pp. 1851-1877.
46. Santhosh, C., Singh, K.R., Sheela, K., Swaroop, T.R., and Sadashiva, M.P.: ‘Regioselective synthesis of 2, 5-disubstituted-1, 3, 4-thiadiazoles and 1, 3, 4-oxadiazoles via alkyl 2-(methylthio)-2-thioxoacetates and alkyl 2-amino-2-thioxoacetates’, The Journal of Organic Chemistry, 2023, 88, (16), pp. 11486-11496
47. Mittal, R.K., Mishra, R., Sharma, V., and Mishra, I.: ‘1, 3, 4-thiadiazole: A versatile scaffold for drug discovery’, Letters in Organic Chemistry, 2024, 21, (5), pp. 400-413.
48. Janowska, S., Khylyuk, D., Gornowicz, A., Bielawska, A., Janowski, M., Czarnomysy, R., Bielawski, K., and Wujec, M.: ‘Synthesis and anticancer activity of 1, 3, 4-thiadiazoles with 3-methoxyphenyl substituent’, Molecules, 2022, 27, (20), pp. 6977.